Spectrochimica Acta Part A: Molecular and Biomolecular Spectroscopy 118 (2014) 162–171

Contents lists available at ScienceDirect

Spectrochimica Acta Part A: Molecular and Biomolecular Spectroscopy

journal homepage: www.elsevier.com/locate/saa

Experimental and DFT studies on the vibrational, electronic spectra and NBO analysis of thiamethoxam

Fang Zhang [a], Yu Zhang [b,*], Haiwei Ni [a], Kuirong Ma [b], Rongqing Li [b]

[a] School of Chemical Engineering, Ningxia University, Ningxia 210094, PR China
[b] Huaian Key Laboratory for Photoelectric Conversion and Energy Storage Materials, Jiangsu Key Laboratory for Chemistry of Low-Dimensional Materials, School of Chemistry and Chemical Engineering, Huaiyin Normal University, Huai'an 223300, Jiangsu, PR China

HIGHLIGHTS

- The FT-IR, FT-Raman spectra and UV–vis of the title compound have been recorded experimentally.
- Optimized geometry, vibrational frequencies are obtained with six DFT methods.
- The complete assignments of the experimental spectra are performed on the basis of PED.
- The HOMO and LUMO energies have been calculated.
- The absorption spectra of the compound were computed both in gas-phase and in H_2O solution.

GRAPHICAL ABSTRACT

DFT study of the structural and spectroscopic properties of thiamethoxam has been reported

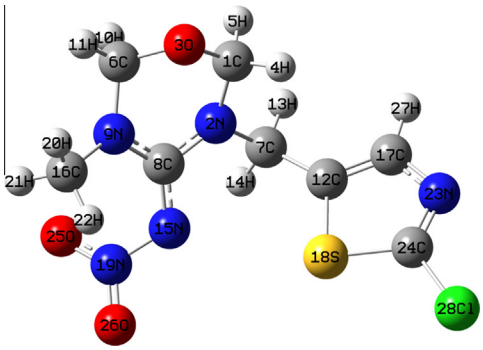

ARTICLE INFO

Article history:
Received 11 June 2013
Received in revised form 8 August 2013
Accepted 15 August 2013
Available online 31 August 2013

Keywords:
Thiamethoxam
Vibrational spectra
Electronic spectra
NBO
Density functional theory (DFT)

ABSTRACT

Vibrational and electronic spectral measurements were performed for 3-(2-chloro-1,3-thiazol-5-ylmethyl)-5-methyl-1,3,5-oxadiazinan-4-ylidene(nitro) amine (thiamethoxam). Optimized geometrical structure and harmonic vibrational frequencies were calculated with *ab initio* RHF and DFT (B3LYP, CAM-B3LYP, M06 and PBE1PBE) methods with 6-311++G (d, p) basis set. Complete assignments of the observed spectra were proposed. The absorption spectra of the compound were computed in gas-phase using TD-B3LYP/6-311++G (d, p) approach and H_2O solution using PCM-TD-B3LYP/6-311++G (d, p) approach. The calculated results matched well with the experimental values. Temperature dependence of thermodynamic parameters in the range of 100–1000 K were determined. The bond orbital occupancies, contribution from parent natural bond orbital (NBO), the natural atomic hybrids was discussed.

Introduction

Neonicotinoids are a class of neuro-active insecticides developed in 1972 by Shell and in 1990s by Bayer [1]. The neonicotinoids were developed in large part because they showed reduced toxicity compared to organophosphate and carbamate insecticides used previously. Because of the different binding affinities with the acetylcholine receptor (nAChR) of insect's neurosystem, they afforded broad spectrum activity and high selectivity [2–4] and much lower toxicity against mammals, birds, aquatic life than insects [5]. Neonicotinoid pesticide is a new group of insecticide class with novel mechanisms of action, which includes the commercial products imidacloprid, acetamiprid, nitenpyram and thiamethoxam [6–8]. Since they became commercially available in 1990s, they were receipted considerable interests from both

* Corresponding author. Tel.: +86 517 83525021; fax: +86 517 83525320.
E-mail address: yuzhang@hytc.edu.cn (Y. Zhang).

1386-1425/$ - see front matter © 2013 Elsevier B.V. All rights reserved.
http://dx.doi.org/10.1016/j.saa.2013.08.076

agricultural chemistry and medicinal fields [9–11]. Thiamethoxam is a representative product of the second-generation neonicotinoid pesticide [12,13]. The compound was introduced to the market in 1991 and has become the world's second largest marketing neonicotinoid with sales of $627 million in at least 65 countries for 115 crops in 2009 [14]. Thiamethoxam affects selectively on the insect nervous system by acting as an agonist at the nicotinic acetylcholine receptors and then blocks the nicotinergic neuronal pathways and attracts amassing of the neurotransmitter acetylcholine [15–19]. It is a very useful insecticide for control of a broad range of sucking insect pests of various crops, such as aphids, plant-hoppers, leaf-hopper and whitefly [20,21]. The unique capabilities of thiamethoxam, such as broad spectrum activity, systemic activity, flexible application methods and low acute mammalian toxicity have resulted in taking place of the organophosphates, carbamates and synthetic pyrethroids [22–24].

Many experimental studies of the toxicities of thiamethoxam have been reported, however, theoretical studies of this compound are scarce, and the mechanisms are still unclear, thus additional studies are required in order to understand the mechanisms involved, which will then facilitate the design of new compound for applications in the biochemical and biophysical fields. In this present work, the efforts have been taken to predict a complete description of the molecular geometry, vibrational frequencies, and natural bond orbital (NBO) analysis. To calculate the absorption spectra, the time-dependent density functional theory (TD-DFT) at B3LYP/6-311++G (d, p) level associated with the polarized continuum model (PCM) was performed. Thermodynamic properties of the title compound at different temperatures have also been calculated and they reveal the correlation between heat capacity, entropy, enthalpy changes, Gibbs free energy and temperatures.

Experimental and computational

Experimental

3-Methyl-4-nitroimino-tetrahydro-1,3,5-oxadiazine (0.1 mol, 16.0 g), 2-chloro-5- (chloromethyl) thiazole (0.12 mol, 20.16 g) and potassium carbonate (0.25 mol, 34.5 g) were dissolved in DMF (100 ml). The mixture was heated for 16 h at 50 °C, then cooled, filtered, and concentrated under vacuum. The product was recrystallized from toluene, giving 21.12 g, yield 72.6%, m.p. 138.5–138.8 °C. ^{1}H NMR (solvent-$CDCl_3$): 7.84 (s, 1H), 4.88 (s, 4H), 4.75 (S, 2H), 3.04 (S, 3H).

The FT-IR of the compound was measured on AVATAR360 spectrophotometer in the range of 400–3500 cm^{-1} at room temperature using KBr pellet technique. The Raman spectra was recorded on Bruker RFS 100/S FT-Raman spectrometer in the 400–3500 cm^{-1} region with diode-pumped air-cooled cw Nd-YAG laser source giving 1064 nm as exciting line at 75 mW power. The UV–vis spectrum was recorded on UV–vis 916 spectrophotometer in the region 200–400 nm using H_2O as solvent.

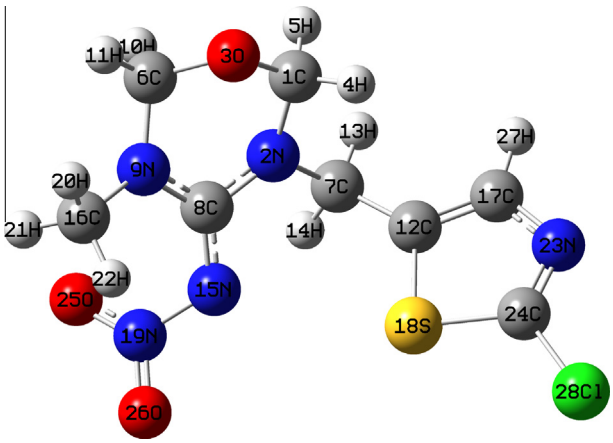

Fig. 1. Optimized geometry with atomic numbering of the title compound.

Methods of calculation

The original geometry of thiamethoxam was optimized using the MM$^+$ molecular modeling in Hyperchem 6.0 package [25]. This equilibrium geometry was then re-optimized at DFT methods B3LYP [26], CAMB3LYP [27], M06 [28], PBE1PBE [29] and *ab initio* RHF method [30] with 6-311++G (d, p) basis set. Time-dependent density functional theory (TD-DFT) [31] excited-state calculation was performed at B3LYP/6-311++G (d, p) level of theory in gas phase. A polarizable continuum model (PCM) [32] including solvent effect was chosen in excitation energy calculations in H_2O solution. All calculations were performed using Gaussian 09W program package [33].

Table 1
Optimized and experimental bond distances (Å) and bond angles (°) for the title compound.

	RHF	B3LYP	CAM-B3LYP	M06	PBE1PBE	Exp[a]
R(1,2)	1.462	1.473	1.466	1.463	1.462	1.471
R(1,3)	1.379	1.402	1.395	1.387	1.392	1.396
R(2,7)	1.459	1.468	1.460	1.457	1.456	1.475
R(2,8)	1.349	1.365	1.358	1.359	1.358	1.337
R(3,6)	1.389	1.419	1.410	1.404	1.408	1.411
R(6,9)	1.442	1.449	1.444	1.442	1.440	1.448
R(7,12)	1.504	1.502	1.498	1.491	1.495	1.495
R(8,9)	1.340	1.358	1.350	1.354	1.351	1.372
R(8,15)	1.313	1.327	1.320	1.318	1.321	1.362
R(9,16)	1.459	1.463	1.457	1.453	1.452	1.462
R(12,17)	1.342	1.365	1.357	1.360	1.364	1.349
R(12,18)	1.743	1.752	1.740	1.742	1.736	1.723
R(15,19)	1.353	1.385	1.375	1.383	1.373	1.330
R(17,23)	1.378	1.375	1.372	1.367	1.367	1.375
R(18,24)	1.728	1.749	1.734	1.742	1.734	1.713
R(19,25)	1.201	1.237	1.228	1.222	1.226	1.254
R(19,26)	1.185	1.222	1.214	1.210	1.213	1.229
R(23,24)	1.264	1.289	1.283	1.285	1.289	1.280
R(24,28)	1.719	1.731	1.722	1.721	1.714	1.717
A(2,1,3)	111.4	111.7	111.5	111.5	111.6	110.8
A(1,2,7)	115.3	115.6	115.6	115.2	115.6	115.3
A(1,2,8)	123.2	122.8	122.9	122.9	122.8	123.1
A(1,3,6)	111.7	110.5	110.4	110.1	110.0	109.0
A(3,6,9)	109.3	109.4	109.3	109.5	109.4	108.7
A(2,7,12)	114.6	114.8	114.4	113.7	114.4	112.4
A(2,8,9)	116.3	115.8	116.0	115.6	115.7	116.9
A(2,8,15)	115.8	116.3	116.2	116.6	116.3	117.3
A(9,8,15)	127.8	127.7	127.7	127.7	127.9	125.3
A(6,9,8)	116.0	115.5	115.4	115.3	115.1	117.9
A(6,9,16)	119.5	120.4	120.4	120.6	120.7	118.5
A(7,12,18)	124.4	123.9	124.0	123.8	123.8	123.6
A(17,12,18)	108.9	109.0	109.2	109.3	109.0	108.8
A(8,15,19)	118.4	118.2	118.0	117.5	117.9	114.9
A(12,17,23)	116.8	116.9	116.7	117.0	116.9	117.1
A(12,18,24)	87.8	87.8	87.9	87.4	88.0	88.4
A(15,19,25)	119.7	119.9	119.7	119.4	119.7	121.0
A(15,19,26)	116.1	115.7	116.0	115.7	115.7	117.7
A(17,23,24)	109.6	109.6	109.6	109.3	109.3	108.5
A(18,24,23)	116.9	116.6	116.7	117.0	116.7	117.1
A(23,24,28)	123.0	123.3	123.2	123.4	123.2	122.9
D(3,1,2,7)	−175.4	−175.7	−174.0	−172.1	−173.6	−169.7
D(1,2,7,12)	77.6	74.8	76.0	74.9	74.4	78.6
D(1,2,8,9)	18.6	23.9	23.0	24.1	24.9	14.7
D(1,3,6,9)	65.2	66.1	66.6	67.3	67.1	66.7
D(2,7,12,18)	67.8	69.4	68.9	68.7	68.9	84.3
D(8,15,19,25)	31.5	30.2	31.8	36.0	30.1	15.9

[a] Ref. [34]

Results and discussion

Molecular geometry

The optimized geometry with atomic numbering scheme for thiamethoxam is given in Fig. 1. The selected experimental bond lengths [34], bond angles and dihedral angles for thiamethoxam are shown in Table 1. It is found that most of the optimized bond lengths are slightly larger than the experimental values, due to that the theoretical calculations belong to isolated molecules in gaseous phase and the experimental results belong to molecules in solid state [34].

In the compound, the experimental bond length of N23—C24 is 1.280 Å [34] which is a typical C=N double bond, and the theoretical value by DFT calculated bond length of the C=N (ca. 1.28 Å) agrees well with the experimental value. The calculated N15—N19 single bond lengths are longer than the experimental value with RHF and all DFT methods, the best results was achieved by RHF method. As a result of our calculations, N19=O25 bond shows typical double-bond characteristic whereas C24—S18 and C24—Cl28 bonds show single-bond characteristic. The calculated and experimental C8=N15 bond length are relatively larger than C24=N23 due to the electron-withdrawing effect depending on the presence of nitro group. The calculated N15N19O26 angle is ca. 116°, about 1.5° smaller than the experimental result. The bond angle value of N23C24Cl28 calculated with DFT methods is ca. 123° which is very close to the experimental result. As shown in Fig. 1, the molecular structure is non-planar, and the plane of the oxadiazine ring forms dihedral angle C1N2C7C12 with thiazole ring being observed at 78.6° in experiment. This dihedral angle was found to be 77.6° and 74.4–76.0° for RHF and DFT method, respectively.

Vibrational assignments

The observed and simulated FT-IR and Raman spectra of thiamethoxam are shown in Figs. 2 and 3, respectively. The calculated theoretical frequencies using RHF and DFT methods (B3LYP, CAM-B3LYP, M06 and PBE1PBE) with 6-311++G (d, p) basis sets, IR intensities and Raman active are listed in Table 2. PEDs were calculated with CAMB3LYP/6-311++G (d, p) theoretical level and listed in Table 2, too. In order to fit the theoretical wavenumbers to the experimental wavenumbers, overall scaling factors have been introduced by using a least-square optimization of the computed to the experimental data. The scale factors are 0.91843 for RHF, 0.96029 for B3LYP, 0.95581 for CAMB3LYP, 0.97052 for M06, and 0.95773 for PBE1PBE theoretical methods. Comparison of the frequencies calculated at all levels with experimental values reveals the overestimation of the calculated vibrational modes due to neglect of anharmonicity in real system. Further, inclusion of electron correlation in DFT methods to certain extend makes the frequency values smaller in comparison with the RHF frequency data.

C—H vibrational modes

In ring R1, an IR band observed at 3085 cm^{-1} and Raman band 3093 cm^{-1} are assigned to C17H stretching vibration, the B3LYP/

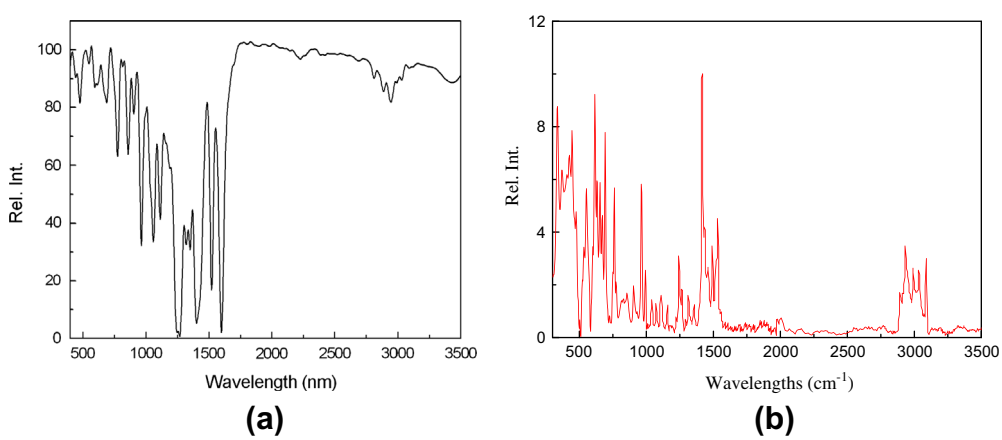

Fig. 2. Experimental FT-IR (a) and FT-Raman (b) spectra for the title compound.

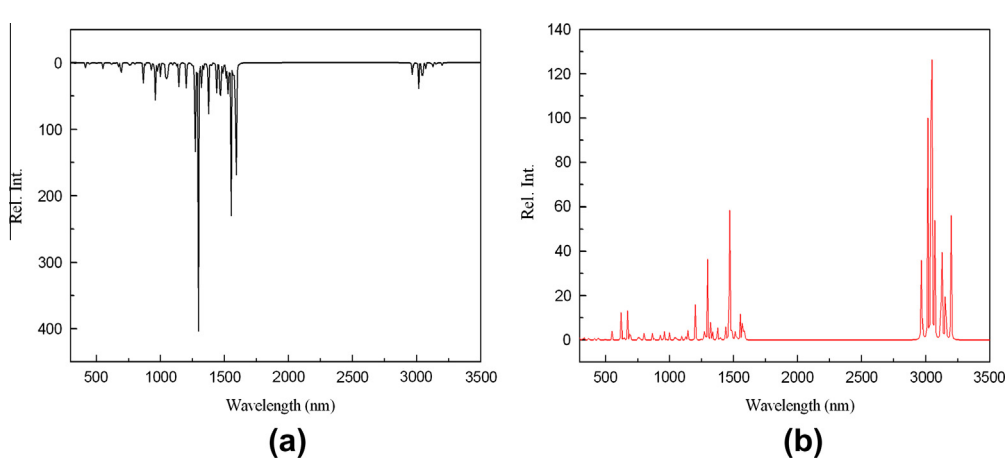

Fig. 3. Calculated IR (a) and Raman (b) spectra for the title compound.

Table 2
Experimental and calculated vibrational frequencies (cm^{-1}) with different methods.

RHF			B3LYP			CAMB3LYP			M06			PBE1PBE			Exp		Assign
Freq	IR Int.	Raman act	Freq	IR Int.	Raman act	Freq	IR Int.	Raman act	Freq	IR Int.	Raman act	Freq	IR Int.	Raman act	IR	Raman	
28	2.5	1.4	27	2.8	1.9	29	2.7	1.9	29	2.3	2.1	28	2.8	2.0			ωC1N2C7H(8) + ωC8N2C7C12(6) + ωC8N2C7H(11)
39	0.1	0.8	36	0.2	1.3	37	0.1	1.0	41	0.1	1.3	36	0.1	1.1			ωC1N2C7H(21) + ωO3C1N2C7 (11) + ωHC7N2C8(11) + ωC7N2C8N(15)
52	2.2	2.1	47	2.1	2.3	49	2.4	2.3	49	2.6	2.2	48	2.3	2.3			ωN2C7C12C17 (20) + ωN2C7C12S18(11)+ωHC7C12C17(37) + ωHC7C12S18(22)
71	1.7	1.1	66	1.4	1.8	67	1.5	1.7	71	1.6	2.1	67	1.4	1.8			ωO3C1N2C8(6) + ωHC1N2C8(11) + ωC1N2C7H(7) + ωC6N9C16H (12)
86	0.4	1.9	80	0.0	1.9	83	0.0	1.9	87	0.0	1.9	83	0.0	1.7			ωO3C1N2C8(9) + ωHC1N2C8(18) + ωHC1O3C6(6) + ωHC6N9C16(10) + ωC8N15N19O(8)
98	4.6	0.5	96	4.6	0.8	98	4.6	0.6	100	4.8	0.4	98	4.6	0.6			ωO3C6N9C16(8) + ωHC6N9C16(16) + ωN2C8N9C16(9) + ωN15C8N9C16(10) + ωC8N9C16H(17)
118	2.3	0.5	108	2.3	0.8	111	2.4	0.7	112	1.3	0.6	112	2.1	0.8			ωO3C1N2C(16) + ωHC1N2C(31) + ωHC1O3C6(11) + ωN2C1O3C6(4) + ωC6N9C16H(9)
152	0.6	0.2	141	1.3	0.4	144	1.1	0.2	146	0.8	0.3	144	1.2	0.3			ωO3C1N2C8(11) + ωHC1N2C(22) + ωHC1O3C6(9) + ωC1N2C7H(9) + ωC1N2C8N9(5)
162	1.9	0.9	152	1.8	1.3	154	1.9	1.3	151	2.0	1.4	154	2.1	1.4			ωC6N9C16H(39) + ωC16N9C6H(18) + ωO3C6N9C16 (9)
204	11.1	0.6	178	2.4	1.1	191	6.8	1.1	193	8.8	1.2	187	4.8	1.2			ωC6N9C16H(50) + ωC8N9C16H(30)
221	0.2	0.4	194	7.2	0.5	209	3.4	0.2	216	1.4	0.9	202	5.0	0.2			ωC8N9C16H(52) + ωC16N9C6H(8)
238	3.6	0.5	216	2.9	0.9	222	2.8	0.8	227	1.9	0.6	221	2.6	0.8			ωC1O3C6H(9) + ωN2C1O3C6 (5) + ωC6N9C16H(9) + ωC8 N9C16H(9) (9)
286	5.5	0.9	262	4.7	1.4	269	5.2	1.1	271	5.1	1.2	268	5.0	1.4			ωC1N2C7H(12)+ωO3C1N2C8(7) + ωHC2N2C8(15) + ωO3C1N2C8(7)
318	3.7	2.3	290	2.5	3.1	298	2.8	2.5	292	3.3	2.9	295	2.4	2.6			δS18C24Cl28 + ωC8N2C7H
																	(9) + ωC8N2C7C12(5) + ωHC7C12C17(14) + ωC12S18C24C28(5) + ωC17N23C24Cl28(5)
346	1.5	2.8	317	1.7	3.5	325	1.8	2.9	329	0.3	3.8	321	1.9	2.8			ωHC6N9C8 + ωC1O3C6H(8) + ωC17N23C24Cl28(5)
361	2.3	2.2	331	2.2	2.4	339	1.9	2.5	354	3.5	1.5	337	1.8	2.8		332	ωC1O3C6O9(4) + ωC1O3C6H(8) + ωC17N23C24Cl28(6)
396	5.1	2.4	364	1.6	3.8	372	2.1	3.3	364	0.9	3.2	369	1.9	3.6			ωC1N2C7H(8) + ωC8N2C7H (24) + ωHC7C12S18(16) + ωC8N2C7C12(24)
441	8.6	0.6	409	7.4	0.7	417	7.4	0.7	421	8.4	1.1	414	6.6	0.7		369	ωC1O3C6O9(6) + ωC1O3C6H(19) + ωHC6N9C8 (19)
474	0.9	0.6	435	0.7	1.3	443	0.6	0.9	445	0.5	1.0	439	0.4	1.0		423	ωC1N2C7H(15) + ωC8N2C7H (13) + ωHC7C12C17 (11) + ωHC7C12S18(19)
484	7.6	3.9	444	8.6	3.0	456	6.8	2.9	450	7.7	2.8	456	7.0	2.7	445	447	νC24Cl28(20) + ωC1N2C7H(11)
539	5.4	1.2	494	4.9	1.2	504	5.4	1.1	497	4.9	1.2	500	5.6	1.1	477	476	ωS18C12C17N23(12) + ωC12S18C24N23(8)
583	0.4	0.6	534	0.3	0.5	547	0.3	0.5	541	0.2	0.8	543	0.3	0.5			ωC8N9C6H(11) + ωS18C12C17N23(6)+C12S18C24N23(6)
598	11.5	4.4	546	13.4	6.2	560	11.7	4.8	555	13.2	5.6	559	11.8	5.3			ωC8N9C16H(11) + ωC6N9C16H(5) + ωHC7C12C17(12)
664	9.3	1.1	607	5.1	0.8	624	5.8	0.7	605	5.2	0.7	616	5.2	0.5		561	ωC12C17N23C24(25) + ωHC17N23C24(17) + ωC17N23C24S18 (23)
676	3.8	7.9	617	2.3	14.2	632	4.2	9.2	623	2.6	14.3	630	4.3	11.9			νC24S18 (8) + νC24SCl28 (3)
702	6.3	4.4	638	5.9	4.9	655	4.0	6.0	646	3.9	4.2	652	3.8	5.9	614	615	νC24S18 (6) + ωHC6N9C16 (10) + ωC6N9C8N15 (5)
716	9.6	9.6	665	5.7	13.6	686	4.6	11.7	677	4.1	13.6	687	2.9	12.1	631	627	νC12S18 (33) + ωC8N2C7H (11)
749	20.8	1.7	681	12.9	2.8	703	16.4	2.5	687	15.8	3.3	697	16.2	3.8		657	ωO3C1N2C(4) + ωC8N2C7H (12) + ωC1N2C8 N9(8) + ωC7N2C8 N15(10) + ωN15C8N9C16(6)
769	9.3	2.2	690	17.7	2.6	708	13.5	2.5	696	15.4	2.4	705	17.3	2.2	673	672	ωHC7C12C17 (9) + ωN2C8N9C6(6) + ωN15C8N9C16(8)
817	4.2	4.1	749	8.7	3.7	768	8.9	3.8	750	5.9	5.7	764	5.7	5.1	693	694	νC24S18 (9) + δC1C17N23(7) + δC12C7N2 (7)
862	33.5	4.4	757	19.8	5.9	778	24.9	6.0	766	25.3	5.2	777	23.4	4.7	745		ωC8N15N19O25(14) + ωN9C8N15N19(18) + ωN15C8N9C16(11) + ωC7N25C8N15(10)
901	17.5	6.4	796	5.4	8.0	817	6.4	7.3	812	6.1	7.4	818	6.7	7.3	775	760	ωC8N15N19O(35) + ωN2C8N15N19(10) + δON19O(8)
955	39.0	1.0	858	37.3	3.7	881	35.9	3.0	862	22.3	1.2	875	28.1	1.5			νC6N9 (4) + ωHC17C12C7(10) + ωHC17C12S18(11) + ωHC17N23C24(9)
992	4.9	2.6	875	4.4	1.0	900	3.8	1.1	874	18.7	2.5	886	10.4	2.3	853		ωHC17C12C7(40) + ωHC17C12S18(26) + ωHC17N23C24(23)
1022	34.2	4.9	920	20.5	4.3	941	25.2	4.2	918	28.9	4.5	931	23.6	4.6			ωHC7N2 C(24) + ωHC7C12C17(25) + ωHC7C12S18(9)
1077	22.7	4.5	952	169.9	11.4	991	138.0	9.7	977	183.3	6.6	993	137.1	11.1	902	904	νO3C6(31) + νN15N19(12) + νC6N9 (5)
1087	85.2	4.7	972	24.3	0.7	1004	26.6	1.2	1000	41.1	5.5	1004	20.2	1.0			νO3C6 (13) + νN15N19(14)
1113	37.5	3.7	994	21.6	3.7	1021	18.4	3.6	1008	8.1	1.2	1018	18.8	4.4	962	964	δHC7C12(11) + ωHC7N2 C(30) + ωHC7C12C17(10)
1158	162.9	2.1	1038	172.2	8.2	1073	57.5	0.7	1040	183.2	11.1	1068	61.8	0.6		994	νC24S18 (24) + νC24Cl28 (26) + δC17N23C24(13) + δN23C24S18(12) + δN23C24Cl28(12)
1161	67.2	0.9	1052	44.8	1.2	1080	168.6	5.7	1058	57.7	0.8	1075	174.6	9.2			νO3C (6) + δHC6N9(10) + δHC16N9(10) + ωHC6N9 C(21) + ωHC6O3 C1(20)
1197	2.7	2.5	1090	2.5	1.7	1113	3.3	1.6	1095	2.6	1.4	1106	4.0	1.4	1034		νC7N2 (4) + νC6N9 (9) + δHC16N9(10) + ωHC1N2 C(19)
1232	4.7	2.0	1120	11.8	5.7	1141	6.9	1.4	1118	7.5	1.2	1134	6.4	1.2	1058		νO3C (14) + δHC1N2(10) + ωHC1N2 C(26)
1243	17.3	10.2	1125	5.2	0.8	1154	4.1	1.5	1128	6.5	1.2	1143	4.6	1.0	1072	1073	νC1O3 (6) + δHC1N2(8) + δHC6N9(12) + ωHC1N2 C(16)
1249	13.8	0.3	1138	35.4	4.2	1160	1.2	4.9	1149	4.6	6.3	1156	0.4	4.3			νC1N2 (9) + νC7C12 (7) + δHC16N9(11)
1269	33.2	13.3	1144	4.5	0.5	1173	35.2	4.4	1160	37.8	2.9	1170	32.4	3.5			δHC16N9(43) + δHC6O3(14) + ωHC16N9 C6(19) + ωHC16N9 C8(18)
1281	16.3	4.7	1194	34.6	15.4	1211	17.0	10.4	1197	19.4	11.1	1211	19.9	10.6	1111	1109	νC17N23(17) + δHC17C12(14) + δHC17N23(33)
1314	29.2	5.9	1198	19.2	3.0	1232	20.0	4.0	1220	14.6	2.4	1233	14.2	2.7	1156	1162	νC1N2(8) + νC7N2(6) + νC7C12(16) + νC17N23(11) + δHC7C12(11)
1365	7.3	3.6	1240	9.0	1.5	1261	13.5	2.9	1241	16.3	3.5	1252	20.6	3.1	1177		δHC1O3(12) + δHC1N2(19) + δHC6O3(14) + ωHC6N9 C8(11)
1391	159.0	4.9	1265	353.8	9.5	1292	156.8	6.0	1270	116.6	7.5	1286	116.5	5.7			δHC1O3(10) + δHC7N2(11) + δHC17C12(8) + δHC17N23(5)
1400	3.9	4.0	1276	6.5	2.5	1301	8.1	3.0	1282	16.3	5.5	1297	16.1	4.3			νC6N9(10) + δHC1N2(6) + δHC1N2(6) + δHC1O3(11) + δHC16N9(15) + ωHC16N9 C6(9)
1435	56.6	5.2	1291	426.4	38.5	1334	125.3	10.9	1311	33.4	7.2	1328	47.9	6.1			νN15N19(10) + νN19O(20) + δHC17C12(13) + δHC17N23(8)
1451	105.0	6.4	1315	35.0	7.8	1342	307.5	17.8	1323	180.9	7.0	1340	218.4	8.8	1241	1242	δO3C1H(8) + δO3C6H(14) + δHC17C12(10) + δHC17N23(6) + ωHC6N9 C (10)
1490	84.5	3.8	1329	22.2	8.8	1358	243.2	32.8	1344	480.4	37.1	1356	408.2	35.2	1269	1265	δO3C6H(16) + δN9C1H(12) + δHC17C12(7) + ωHC6N9 C (9)

(*continued on next page*)

Table 2 (*continued*)

RHF			B3LYP			CAMB3LYP			M06			PBE1PBE			Exp		Assign
Freq	IR Int.	Raman act	Freq	IR Int.	Raman act	Freq	IR Int.	Raman act	Freq	IR Int.	Raman act	Freq	IR Int.	Raman act	IR	Raman	
1498	30.7	2.4	1367	36.1	8.2	1388	60.3	3.9	1358	0.5	5.1	1376	4.0	4.3	1313	1307	δN2C1H(12) + δN9C6H(12) + δHC7C12(12) + ωHC7C12 C17 (16)
1510	660.9	31.6	1370	104.5	6.3	1391	105.3	9.3	1362	137.4	6.6	1380	135.1	8.0	1326		δN2C1H(11) + δN2C1H(12) + δO3C6H(16) + δN9C6H(16)
1530	218.5	14.8	1391	19.7	6.1	1412	7.8	4.6	1379	31.8	9.1	1399	21.4	8.1	1350	1361	δHC7N2(29) + δHC7C12(26)
1574	152.3	6.2	1434	80.1	10.2	1452	73.6	8.5	1413	24.4	15.9	1439	70.2	10.4	1398		δHC6O3(13) + δHC1O3(13) + δHC16N9(11) + δHC16H(12)
1597	27.6	11.1	1459	32.5	15.6	1471	24.3	12.9	1418	70.1	9.4	1449	23.3	13.6			δHC7H(32) + ωHC7N2C1(15) + ωHC7N2C8(14)
1604	69.5	8.6	1462	63.4	10.3	1477	44.3	4.2	1445	26.4	5.9	1462	42.8	5.2			δHC16H(15) + δHC16N9(23)
1622	25.6	11.6	1468	64.8	88.6	1496	20.8	11.9	1470	25.5	15.6	1480	14.3	12.2	1413	1415	νN23C24(41) + νC12C17(9) + νC24Cl28(6)
1633	20.5	3.4	1485	38.8	8.8	1513	82.8	90.0	1475	13.2	4.0	1500	22.1	28.4			δHC16H(53) + ωHC16N9C6(20) + ωHC16N9C8(20)
1645	85.9	75.6	1506	31.1	5.2	1516	19.6	3.8	1488	16.6	9.2	1502	83.6	75.1	1433	1427	δHC10H(32) + ωHC6N9C8(15) + ωHC6N9C11(16)
1651	56.5	8.3	1513	18.7	3.6	1523	16.7	4.3	1493	32.5	32.8	1510	17.5	4.0			δHC16H(50) + ωHC6N9C16(18) + ωHC8N9C16(18)
1671	150.9	9.1	1526	163.5	3.4	1541	41.3	5.6	1495	80.8	68.6	1527	22.3	6.9		1487	δHC1H(25) + δHC1O3(8) + ωHC1N2C7(17) + ωHC1N2C7(17)
1693	499.5	13.6	1546	300.1	15.0	1583	522.3	9.9	1565	501.7	5.4	1583	464.0	8.8		1488	νN19OC7(9) + δHC1H(27) + ωHC1O3C6(17)
1720	428.9	6.6	1566	59.1	37.0	1613	4.6	30.3	1589	4.3	40.7	1599	31.8	32.1			νC12C17(25) + νC12C7(7) + νC12C7(7) + νN19OC7(9) + δHC17C27(13) + δHC17N23(19)
1756	15.5	22.6	1577	90.7	12.9	1619	261.2	7.9	1603	439.8	4.1	1624	336.2	6.8	1520		νC8N2(9) + νC8N15(9) + νN19O26(10) + δHC1H(7) + δN2C1H(5)
1771	709.3	5.4	1585	539.9	2.4	1633	567.8	7.6	1647	384.3	11.6	1647	458.6	11.2	1527	1535	νC8N9(20) + νC8N19(11)+δN9C6H(6)+δHC6H(7) + δHC16H(20)
3156	57.1	79.7	2968	66.2	137.2	3001	58.9	127.9	2935	68.0	135.4	2986	66.1	141.9	2816		νC1H(98)
3185	57.9	85.4	3013	45.4	117.2	3041	39.2	106.6	2987	47.0	109.4	3033	42.5	114.3	2890	2901	νC6H(98)
3202	34.0	150.1	3039	26.5	144.0	3070	22.4	155.9	3025	23.3	125.8	3061	24.4	175.7			νC7H(98)
3207	33.7	124.3	3045	26.2	176.0	3071	21.1	131.3	3036	29.3	150.8	3062	23.1	144.2	2933	2925	νC16H(99)
3261	23.1	66.8	3069	14.8	93.9	3102	12.1	81.6	3040	14.4	105.2	3087	12.9	90.0	2951	2943	νC1H(98)
3273	15.4	52.9	3115	7.3	56.9	3145	5.2	52.3	3111	0.5	59.3	3141	4.7	52.5			νC16H(98)
3296	7.1	25.8	3123	0.3	62.8	3152	4.8	23.5	3119	5.9	48.1	3145	0.1	58.6			νC7H(98)
3309	0.8	50.5	3126	5.7	24.6	3154	0.1	52.9	3125	6.6	72.0	3151	6.0	28.2	2991	2997	νC16H(96)
3320	21.6	97.4	3154	12.4	110.9	3179	9.7	102.0	3132	10.1	55.6	3174	11.1	107.7	3035	3027	νC6H(97)
3366	10.1	92.6	3197	7.1	109.2	3222	6.5	101.1	3173	9.4	102.6	3218	6.6	107.0	3085	3093	νC17H(99)

6-311++G (d, p) calculated values is 3197 cm^{-1}. PED analysis found that this mode is almost pure CH stretching vibration (PED, 99%). An IR band observed at 1111 cm^{-1} and corresponding Raman band at 1109 cm^{-1} are assigned to C17H bending mode (PED, 47%) and coupled with C17N23 stretching mode, The wagging out of plane C17H vibrational mode is observed at 853 cm^{-1}, which is the mixed vibration of HC17C12C7 (PED, 40%), HC17C12S18 (PED, 26%) and HC17N23C24 (PED, 23%).

In ring R2, the vibrational frequencies corresponding to C6H are significantly higher than that of C1—H. The IR band observed at 3035 and 2890 cm^{-1} and Raman bands 3027 and 2901 cm^{-1} are assigned to C6H stretching vibrational modes, the B3LYP calculated values are 3154 and 3013 cm^{-1}, the PED of these modes are 97% and 98%, respectively. The corresponding vibration of C1H are observed at 2951 in IR and 2943 cm^{-1} in Raman spectra these modes are almost pure CH vibrational modes too, PED is 98% for each mode. The IR band observed at 1433 cm^{-1} and corresponding Raman band at 1427 cm^{-1} are assigned to C10H bending modes, this mode is coupled with HC6N9C8 (PED, 15%) and HC6N9C11 (PED, 16%) wagging out of plane vibrational modes. The other C6H bending modes are observed at 1398, 1326 and 1269 cm^{-1} in IR, the first is coupled with bending modes of C16H, the second is coupled with N2C1H (PED, 23%) and the third is coupled with C1H and C17H bending modes. The bending mode of C1H is observed at 1177 cm^{-1} at IR spectra; this band is coupled with C6H bending (PED, 14%) and HC6N9C8 wagging out of plane vibrational modes (PED, 11%). The observed vibrational band at 1072 cm^{-1} in IR spectra and at 1073 cm^{-1} in Raman spectra is assigned to the wagging out of plane vibrational mode, this mode is coupled with the stretching vibrational modes of C1O3 (PED, 6%) and C1H wagging out of plane mode. The other wagging out of plane modes is observed at 1058 cm^{-1} and 1034 cm^{-1}, the former is strongly coupled with C1O3 and C6O3 stretching vibrational mode (PED, 14%) and the later is strongly coupled with C16H bending mode and C—N stretching vibrational mode.

The asymmetry and symmetry C16H stretching vibrational modes is observed at 2991 and 2933 cm^{-1} in IR spectra and 2997 and 2925 cm^{-1} in Raman spectra, respectively, these band are almost pure C-H stretching modes. With B3LYP method, the calculated values of these modes are 2991 and 2924 cm^{-1} (scaled with scale factor 0.96029), respectively. This assignments is corresponding with Gunasekaran's assignments in the compound Levofloxacin [35]. There is no experimental data can be assigned to C16H bending and wagging vibrational modes. The calculated HC16H bending modes are 1453 and 1426 cm^{-1} (scaled) at B3LYP/6–311++G (d, p) theoretical level, the PED for these two modes are more than 50%. The calculated HC16 N bending mode is 1099 cm^{-1} (scaled) at the same level, the mode is strongly coupled with HC6O3 bending mode (PED, 14%) and wagging out of plane HC16N9C (PED, 37%).

There is no experimental data can be assigned to C7H stretching vibrational modes. The calculated C7H stretching modes are 2999 and 2918 cm^{-1} (scaled) at B3LYP/6-311++G (d, p) theoretical level, the PED for these two modes are both 98%. The experimental data 1350, 1313 and 1241 cm^{-1} in IR spectra can be assigned to the C7H bending modes, the first is the mixed bending vibration of HC7N2 (PED, 29%) and HC7C12 (PED, 26%), the second is coupled with N9C6H bending mode and HC7C12C17 wagging out of plane vibrational mode and the third is coupled with bending modes of C6—H and C17—H. The experimental data 962 cm^{-1} in IR spectra and 964 cm^{-1} in Raman spectra can be assigned to the C7H wagging out of plane mode, the mode is the mixed with HC7C12 bending mode (PED, 11%).

Compared with the experimental values, the RHF method overestimates the frequencies with an error 9.3–16.9%, the B3LYP method overestimates the frequencies with an error 2.6–6.0%, and the CAMB3LYP methods overestimate the frequencies with

errors less than 2.9–8.1%. The M06 and PBE1PBE methods overestimate the frequencies with errors 1.1–6.6% and 3.6–8.0%, respectively.

Table 3
The energy levels (eV) of the frontier orbital of the title compound.

	B3LYP	CAMB3LYP	M06	PBE1PBE	HF
LUMO+6	−0.0237	0.8517	−0.6111	0.0103	1.8546
LUMO+5	−0.2071	0.6628	−0.8503	−0.0827	1.6179
LUMO+4	−0.2898	0.5638	−0.9513	−0.1905	1.5714
LUMO+3	−0.4122	0.2781	−1.2130	−0.4895	1.4089
LUMO+2	−0.7622	−0.0634	−1.2587	−0.6996	1.1757
LUMO+1	−1.4906	−0.1246	−1.5208	−1.4315	1.0201
LUMO	−1.9398	−0.5975	−1.7597	−2.0277	0.7034
HOMO	−7.1478	−8.6174	−7.3785	−7.3081	−9.9404
HOMO−1	−7.2697	−8.9167	−7.6207	−7.3951	−10.7444
HOMO−2	−7.6351	−9.2332	−8.0237	−7.6928	−10.9610
HOMO−3	−7.9377	−9.6378	−8.3788	−7.8890	−11.1860
HOMO−4	−8.2618	−9.8585	−8.5752	−8.3366	−11.9019
HOMO−5	−8.3208	−9.9714	−8.6449	−8.5214	−11.9215
HOMO−6	−8.3459	−10.0462	−8.9094	−8.5532	−12.1493

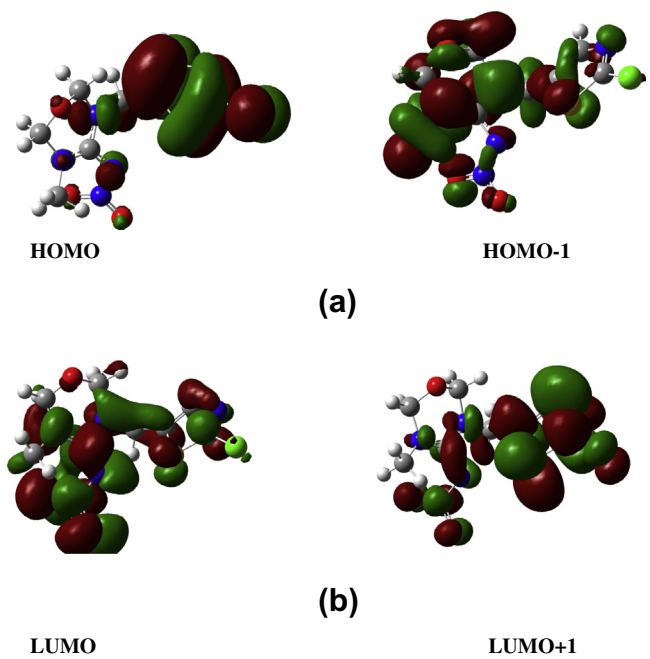

Fig. 4. 3D plots of (a) the HOMO, HOMO-1 and (b) LUMO, LUMO + 1 of pymetrozine molecule.

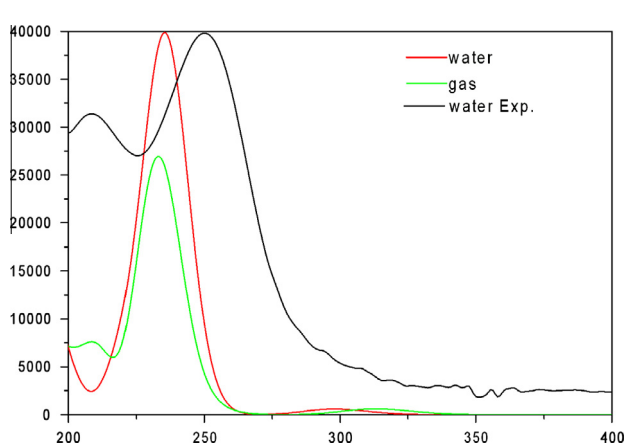

Fig. 5. The experimental and simulated spectra for the title compound.

Ring modes

In the ring R1, the C17—N23 stretching vibration is observed at 1413 cm^{-1} in IR spectra and 1415 cm^{-1} in Raman spectra. The band is coupled with C12C17 and C24Cl28 stretching vibrational modes (PED, 15%) and HC16H bending mode (PED, 12%). The observed band at 631 cm^{-1} in IR spectra and 627 cm^{-1} in Raman spectra are assigned to C12S18 stretching vibration (PED, 33%) which is coupled with C8N2C7H wagging out of plane vibrational mode (PED, 11%). The IR band at 693 cm^{-1} and the corresponding Raman bands at 694 cm^{-1} are assigned to C24S18 stretching vibrational mode, however, the PED of this mode is small. The observed bands at 477 cm^{-1} in the IR spectrum and 476 cm^{-1} in Raman spectra are assigned to the wagging modes of ring R1. For above vibrational modes, computed frequencies at all the levels are higher than that of the experimental ones, the best value was achieved by B3LYP.

The ring C=N and C=C stretching vibrations occur in the region of 1600–1500 cm^{-1}[36] and 1625–1400 cm^{-1}[37], respectively. Almost the C=N and C=C stretching vibrations are found overlapped in the same region and difficult to be assigned.

In the ring R2, the C8—N stretching vibration is observed at 1527 cm^{-1} in IR spectra and 1535 cm^{-1} in Raman spectra (PED,

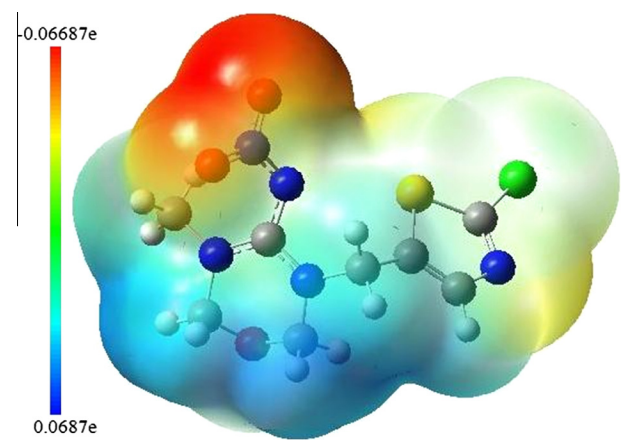

Fig. 6. The negative (red and yellow) regions of MEP are related to nucleophilic recognition and the positive (blue) ones to electrophilic recognition. (For interpretation of the references to color in this figure legend, the reader is referred to the web version of this article.)

Table 4
Thermodynamic properties at different temperatures at B3LYP/6-311++G (d, p) level of the title compound.

T (K)	Cv (cal/Mol K)	*S* (cal/Mol K)	*H* (kcal/mol)	*G* (kcal/mol)
100	29.9	91.6	115.1	115.1
150	39.1	106.3	116.9	101
200	48.1	119.3	119.2	95.3
250	57.2	131.5	121.9	89
298.15	65.9	142.7	125.0	82.4
350	74.7	154.2	128.7	74.7
400	82.6	165.0	132.8	66.7
450	89.7	175.4	137.2	58.2
500	96.0	185.4	142.0	49.2
550	101.6	195.0	147.0	39.7
600	106.5	204.2	152.3	29.7
650	110.9	213.1	157.8	19.2
700	114.9	221.6	163.6	8.3
750	117.4	229.8	169.5	−3
800	121.6	237.6	175.6	−14.7
850	124.1	245.2	181.9	−26.7
900	127.0	252.5	188.3	−39.2
950	129.3	259.5	194.8	−52
1000	131.5	266.3	201.4	−65.2

31%). The band is coupled with the bending vibrational mode of C6H (PED, 13%) and bending vibrational modes (PED, 20%). The observed band at 902 cm^{-1} in IR and 904 cm^{-1} in Raman spectra is assigned to C6O3 stretching vibration which is coupled with N15N19 and C6N9 stretching vibrational mode. For above vibrational modes, computed frequencies at all the levels are higher than that of the experimental ones. The best value was achieved by B3LYP, Compared with the experimental values, the RHF method overestimates the frequencies with an error 13.2–19.4%, the B3LYP method overestimates the frequencies with an error 1.6–5.5%, and the CAMB3LYP methods overestimate the frequencies with errors less than 6.1–8.7%. The M06 and PBE1PBE methods overestimate the frequencies with errors 3.9–8.4% and 4.9–10.1%, respectively.

—NO2 modes

The N—O stretching vibrations in nitroalkanes occur near 1550 cm^{-1} (asymmetrical) and 1365 cm^{-1} (symmetrical). If the nitro group is attached to an aromatic ring, the N—O stretching bands shift to down to slightly lower wavenumbers: 1550–1475 cm^{-1} and 1360–1290 cm^{-1}[38]. The stretching vibration of N19—O appears at 1520 cm^{-1} in the IR spectrum, the band is strongly coupled with C—N stretching modes in the ring 2. The wagging out of plane vibrational mode of N19—O appears at 775 cm^{-1} in the IR spectrum and 760 cm^{-1} in Raman spectrum. The another band 745 cm^{-1} in IR spectrum can also be assigned to the wagging out of plane vibrational mode of N19—O, the band is strongly coupled with the wagging out of plane mode of R2. Compared with the experimental values, the RHF method overestimates the frequencies with an error 15.5–18.5%, the B3LYP method overestimates the frequencies with an error 1.6–4.7%, and the CAMB3LYP methods overestimate the frequencies with errors less than 4.4–7.5%. The M06 and PBE1PBE methods overestimate the frequencies with errors 2.8–6.8% and 4.3–7.6%, respectively.

C—Cl mode

The stretching vibration of C24—Cl28 appears at 445 cm^{-1} in the IR spectrum and 447 cm^{-1} in the Raman spectrum, this is agreement with the literature data [39,40]. The band is strongly coupled with C1N2C7H(11) wagging out of plane modes in the ring 2. There is no experimental data can be assigned to C24Cl28 bending vibrational modes. The calculated frequencies for this mode is 278 cm^{-1} (scaled) at B3LYP/6-311++G (d, p) theoretical level, however, the PED for these two modes is only 10%.

Electronic spectra

Molecular orbital can provide insight into the nature of reactivity, and some of the structural and physical properties of molecules. The energy gap between HOMO and LUMO is a critical parameter in determining molecular electrical transport properties. The calculated energy gap of HOMO–LUMO's explains the ultimate charge transfer interface within the molecule. The energy levels of the frontier orbital of the compound are listed in Table 3. The 3D plots of the HOMO, HOMO−1 and LUMO, LUMO+1 of the compound are shown in Fig. 4. The experimental and simulated spectra are shown

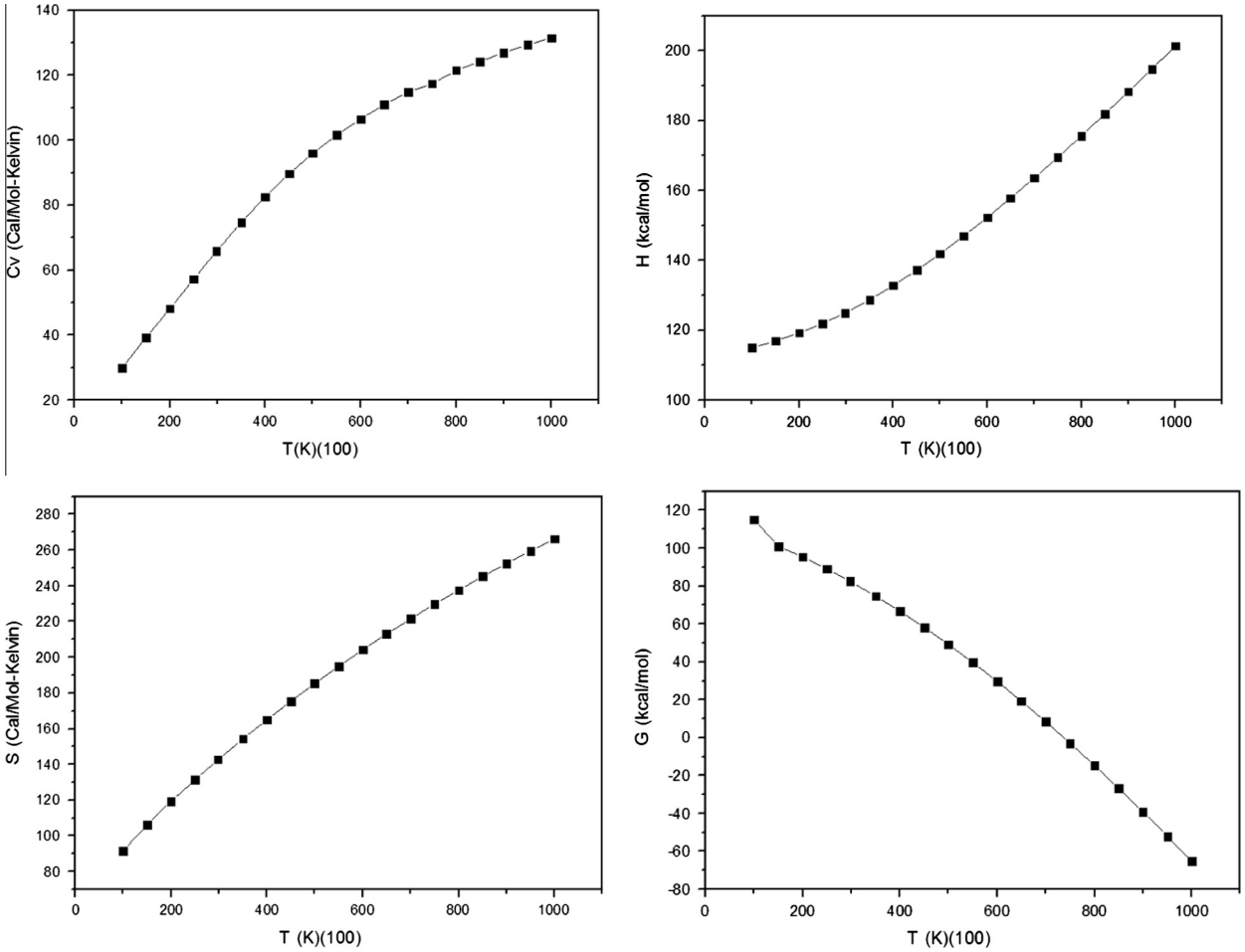

Fig. 7. The correlation of heat capacity (Cv), entropy (*S*), enthalpy (*H*) and Gibbs free energy (*G*) with temperature.

in Fig. 5. According to the B3LYP/6-311++G (d, p) method, the energy level of the highest occupied molecular orbital (E_{HOMO}) is about −7.1 eV and the lowest unoccupied molecular orbital (E_{LUMO}) is about −1.9 eV. As a result, the $E_{HOMO} - E_{LUMO}$ gap in the compound is about 5.2 eV. For the compound, the LUMO and LUMO + x (x: 0–6) energies predicted by the DFT method were quite low (−1.9398 to −0.0237 eV with B3LYP/6-311++G (d,p)), and are therefore excellent electron acceptors, indicating that their interaction with the base-pairs of some insects should be quite strong. Transition state transition of π–π^* type is observed with regard to the molecular orbital theory. The calculated absorption spectrum with B3LYP/6-311++G (d, p) method in gas phase showed band with peaks at 211.8, 238.8 and 323.7 nm matching well with the corresponding experimental absorptions at 208.9, 250.5 nm, respectively. The excited state lies at 211.8 nm are mainly formed by the H−4 → L+1 transition. The excited state located at 238.8 nm is given by the H−4 → L and H−1 → L+1 transition. The excited state located at 323.7 nm is given by the H → L and H−1 → L transitions.

Though the simulated spectrum of the title compound in the gas phase has given a reasonable agreement on the band maximum positions with the experiment results, the calculation including solvent effect was also carried out with the expectation of a better match-up between the simulated and the experimental results. On the basis of the optimized geometry in H_2O solution, the excited states were obtained by the application of TDDFT-B3LYP/6-311++G (d, p) theoretical level in combination with PCM to reproduce a solvent effect. The simulated spectrum in solution also shows three maximum bands centered at 235.6 nm and 298.5 nm. Contrary to the expectation, the simulated spectrum with inclusion of the solvent effect did not give a better match-up result to the experimental. This may be due to the interactions between the thiamethoxam molecules and solvent molecules.

Molecular electrostatic potential

The molecular electrostatic potential (MEP) is best suited for identifying sites for intra- and intermolecular interactions [41,42]. In drug-receptor, it is a very useful descriptor in understanding sites for electrophilic and nucleophilic reactions as well as hydrogen bonding interactions [42]. To predict reactive sites for the investigated pymetrozine molecule, MEP was calculated with B3LYP/6-311++G (d, p) optimized geometry. The negative (red and yellow) regions of MEP are related to nucleophilic recognition and the positive (blue) one to electrophilic recognition shown in Fig. 6. Negative regions in the studied molecule are found around the O25 and O26 atoms indicating a possible site for nucleophilic attack. According to these calculated results, the MEP map shows that the negative potential sites are on electronegative atoms as well as the positive potential sites are around the hydrogen atoms. These sites give information about the region from where the compound can have noncovalent interactions. For the MEP surface in the studied molecule the negative region associated with O25 and O26 atoms and also the weak positive region by the nearby H22 atom are indicative of a weak intramolecular (N19—O25···H22 2.449 Å) hydrogen bonding [43]. Thus the compound provides higher binding opportunity for the receptor molecule, such as proteins without any steric hindrance posed by amino acid chains of receptor.

Thermodynamic properties

The temperature dependence of the thermodynamic properties heat capacity at constant volume (Cv), entropy (S), enthalpy (H) and Gibbs free energy (G) for the title compound were also determined by B3LYP/6-311++G (d, p) method and are listed in Table 4. It can be observed that these thermodynamic functions are increasing with temperature ranging from 100 to 1000 K due to the fact that the molecular vibrational intensities increase with temperature [44]. The correlation equations between heat capacity, entropy, enthalpy and Gibbs free energy with temperatures were filled by quadratic formulas, and the corresponding fitting factors (R^2) for these thermodynamic properties are 0.99931, 0.99987, 0.99928 and 0.9995, respectively. The corresponding fitting equations are as follows and the correlation graphs were shown in Figs. 7.

Table 5
The calculated atomic orbital occupancies and energy with B3LYP /6-311++G (d, p) theoretical level.

Atom	Type(AO)	Occ.	Energy	Atom	Type(AO)	Occ.	Energy
C1	Cor(1S)	1.99922	−10.18003	C17	Cor(1S)	1.99891	−10.08785
	Val(2S)	0.98113	−0.27791		Val(2S)	0.91818	−0.18488
	Val(2px)	0.97463	−0.14172		Val(2px)	0.93345	−0.07564
	Val(2py)	0.89347	−0.12371		Val(2py)	1.12800	−0.11006
	Val(2pz)	0.94183	−0.12617		Val(2pz)	1.01964	−0.12430
N2	Cor(1S)	1.99926	−14.22422	S18	Cor(1S)	2.00000	−87.71191
	Val(2S)	1.21701	−0.56844		Cor(2S)	1.99907	−8.88060
	Val(2px)	1.46993	−0.29358		Val(3S)	1.65226	−0.77770
	Val(2py)	1.31692	−0.29384		Cor(2px)	1.99984	−5.94687
	Val(2pz)	1.48045	−0.29003		Val(3px)	1.04533	−0.20912
O3	Cor(1S)	1.99977	−18.98248		Cor(2py)	1.99985	−5.94433
	Val(2S)	1.62477	−0.91584		Val(3py)	1.34723	−0.23095
	Val(2px)	1.41113	−0.33309		Cor(2pz)	1.99992	−5.94415
	Val(2py)	1.81164	−0.35143		Val(3pz)	1.43564	−0.24929
	Val(2pz)	1.70576	−0.35864	N19	Cor(1S)	1.99959	−14.42332
H4	Val(1S)	0.80264	−0.01306		Val(2S)	1.05792	−0.51484
H5	Val(1S)	0.83748	−0.03334		Val(2px)	1.06087	−0.28137
C6	Cor(1S)	1.99923	−10.17635		Val(2py)	1.07062	−0.27784
	Val(2S)	0.97974	−0.27398		Val(2pz)	1.16455	−0.31451
	Val(2px)	0.89238	−0.13809	H20	Val(1S)	0.80028	−0.00511
	Val(2py)	0.77020	−0.10747	H21	Val(1S)	0.77784	0.02303
	Val(2pz)	1.17086	−0.15244	H22	Val(1S)	0.78246	0.00854
C7	Cor(1S)	1.99910	−10.11545	N23	Cor(1S)	1.99920	−14.13598
	Val(2S)	0.98639	−0.25170		Val(2S)	1.38243	−0.55163
	Val(2px)	0.93620	−0.11714		Val(2px)	1.51069	−0.22636
	Val(2py)	1.23024	−0.14869		Val(2py)	1.34955	−0.23144
	Val(2pz)	1.02663	−0.13380		Val(2pz)	1.21196	−0.20403
C8	Cor(1S)	1.99912	−10.19117	C24	Cor(1S)	1.99905	−10.20134
	Val(2S)	0.71791	−0.13576		Val(2S)	0.99555	−0.32982
	Val(2px)	0.83667	−0.08429		Val(2px)	0.98710	−0.22113
	Val(2py)	0.87335	−0.08084		Val(2py)	0.96256	−0.14846
	Val(2pz)	0.86522	−0.13587		Val(2pz)	1.02392	−0.19331
N9	Cor(1S)	1.99923	−14.22058	O25	Cor(1S)	1.99979	−18.93163
	Val(2S)	1.20623	−0.55929		Val(2S)	1.75948	−0.90087
	Val(2px)	1.44379	−0.29047		Val(2px)	1.31723	−0.25807
	Val(2py)	1.31123	−0.28613		Val(2py)	1.86903	−0.28695
	Val(2pz)	1.50567	−0.28739		Val(2pz)	1.48108	−0.27399
H10	Val(1S)	0.82312	−0.02948	O26	Cor(1S)	1.99978	−18.92652
H11	Val(1S)	0.79720	−0.02044		Val(2S)	1.75006	−0.89364
C12	Cor(1S)	1.99895	−10.10763		Val(2px)	1.75796	−0.27605
	Val(2S)	0.98126	−0.26867		Val(2py)	1.36573	−0.25520
	Val(2px)	1.08797	−0.12235		Val(2pz)	1.49223	−0.26991
	Val(2py)	1.05179	−0.17000	H27	Val(1S)	0.79120	0.01407
	Val(2pz)	1.11072	−0.17080	Cl28	Cor(1S)	2.00000	−100.22125
H13	Val(1S)	0.78373	−0.01174		Cor(2S)	1.99962	−10.51574
H14	Val(1S)	0.74753	0.02190		Val(3S)	1.83363	−1.02970
N15	Cor(1S)	1.99923	−14.18187		Cor(2px)	1.99995	−7.24674
	Val(2S)	1.41505	−0.55332		Val(3px)	1.57645	−0.31604
	Val(2px)	1.47162	−0.22446		Cor(2py)	1.99996	−7.24414
	Val(2py)	1.08827	−0.18730		Val(3py)	1.77586	−0.32685
	Val(2pz)	1.47795	−0.22685		Cor(2pz)	1.99996	−7.24484
C16	Cor(1S)	1.99929	−10.09652		Val(3pz)	1.72318	−0.32575
	Val(2S)	1.07220	−0.27667				
	Val(2px)	1.15537	−0.13074				
	Val(2py)	1.07625	−0.12320				
	Val(2pz)	1.04231	−0.11857				

Table 6
Bond orbital analysis of title compound with B3LYP/6-311++G (d, p) level of theory.

Bond	Occupancy	Atom	Contribution from parent NBO (%)	Atomic hybrid contributions (%)		Hybrid
				s	p	
C1—N2	1.98421	C1	36.23	24.61	75.24	$sp^{3.06}$
		N2	63.77	30.20	69.77	$sp^{2.31}$
C1—O3	1.98983	C1	33.00	22.67	77.04	$sp^{3.40}$
		O3	67.00	28.32	71.61	$sp^{2.53}$
C1—H4	1.98112	C1	60.26	26.44	73.49	$sp^{2.78}$
		H4	39.74	99.96	0.04	$sp^{0.00}$
C1—H5	1.98785	C1	58.89	26.44	73.49	$sp^{2.78}$
		H5	41.11	99.96	0.04	$sp^{0.00}$
N2—C7	1.98003	N2	63.39	32.50	67.48	$sp^{2.08}$
		C7	36.61	22.10	77.76	$sp^{3.52}$
N2—C8	1.97844	N2	62.09	36.03	63.92	$sp^{1.77}$
		C8	37.91	30.99	68.90	$sp^{2.22}$
O3—C6	1.98817	O3	67.57	27.39	72.54	$sp^{2.65}$
		C6	32.43	21.74	77.96	$sp^{3.59}$
C6—N9	1.98583	C6	36.63	25.36	74.50	$sp^{2.94}$
		N9	63.37	31.10	68.87	$sp^{2.21}$
C6—H10	1.98662	C6	59.49	26.52	73.40	$sp^{2.77}$
		H10	40.51	99.96	0.04	$sp^{0.00}$
C6—H11	1.98461	C6	60.23	26.50	73.44	$sp^{2.77}$
		H11	39.77	99.95	0.05	$sp^{0.00}$
C7—C12	1.98104	C6	49.33	30.60	69.36	$sp^{2.27}$
		C12	50.67	36.59	63.38	$sp^{1.73}$
C7—H13	1.96993	C7	60.75	23.07	76.87	$sp^{3.33}$
		H13	39.25	99.96	0.04	$sp^{0.00}$
C7—H14	1.97328	C7	62.64	24.34	75.59	$sp^{3.11}$
		H14	37.36	99.96	0.04	$sp^{0.00}$
C8—N9	1.98087	C8	38.50	33.31	66.59	$sp^{2.00}$
		N9	61.50	34.85	65.10	$sp^{1.87}$
C8—N15	1.97932	C8	42.65	35.36	64.56	$sp^{1.83}$
		N15	57.35	37.24	62.67	$sp^{1.68}$
C8—N15	1.84888	C8	27.22	0.27	99.40	$sp^{99.99}$
		N15	72.78	0.34	99.53	$sp^{99.99}$
N9—C16	1.98586	N9	64.45	33.54	66.43	$sp^{1.98}$
		C16	35.55	23.18	76.68	$sp^{3.31}$
C12—C17	1.98392	C12	51.00	39.05	60.91	$sp^{1.56}$
		C17	49.00	38.90	61.06	$sp^{1.57}$
C12—C17	1.87795	C12	54.29	0.01	99.94	$sp^{1.00}$
		C17	45.71	0.01	99.92	$sp^{1.00}$
C12—S18	1.96739	C12	52.25	24.28	75.53	$sp^{3.11}$
		S18	47.75	18.25	81.14	$sp^{4.45}$
N15—N19	1.98600	N15	45.32	21.86	78.00	$sp^{3.57}$
		N19	54.68	32.48	67.44	$sp^{2.08}$
C16—H20	1.98850	C16	59.99	25.08	74.86	$sp^{2.98}$
		H20	40.01	99.96	0.04	$sp^{0.00}$
C16—H21	1.98831	C16	61.33	26.35	73.59	$sp^{2.79}$
		H21	38.67	99.96	0.04	$sp^{0.00}$
C16—H22	1.98884	C16	60.91	25.47	74.47	$sp^{2.92}$
		H22	39.09	99.96	0.04	$sp^{0.00}$
C17—N23	1.96769	C17	40.44	29.50	0.44	$sp^{2.39}$
		N23	59.56	31.83	67.96	$sp^{2.13}$
C17—H27	1.97547	C17	60.61	31.59	68.36	$sp^{2.16}$
		H27	39.39	99.94	0.06	$sp^{0.00}$
S18—C24	1.98131	S18	46.24	15.81	83.54	$sp^{5.28}$
		C24	53.76	33.06	66.75	$sp^{2.02}$
N19—O25	1.99559	N19	49.63	33.69	66.18	$sp^{1.96}$
		O25	50.37	23.45	76.41	$sp^{3.26}$
N19—O26	1.99479	N19	49.28	32.24	67.62	$sp^{2.10}$
		O26	50.72	23.58	76.28	$sp^{3.24}$
N19—O26	1.98921	N19	39.80	1.45	98.28	$sp^{67.68}$
		O26	60.20	0.92	98.93	$sp^{99.99}$
N23—C24	1.99093	N23	59.57	37.79	61.99	$sp^{1.64}$
		C24	40.43	38.53	61.43	$sp^{1.59}$
N23—C24	1.89424	N23	54.61	0.00	99.76	$sp^{1.00}$
		C24	45.39	0.00	99.93	$sp^{1.00}$
C24—Cl28	1.98842	C24	47.44	28.26	71.54	$sp^{2.53}$
		Cl28	52.56	17.10	82.35	$sp^{4.82}$

Table 7
Global and local reactivity descriptors and related molecular properties of calculated values.

Molecular Properties	RHF	B3LYP	CAM-B3LYP	M06	PBE1PBE
Ionization potential (I)	0.35613	0.26269	0.31670	0.27117	0.26904
Electron affinity (A)	−0.02469	0.07129	0.02196	0.06467	0.05932
Global hardness(η)	0.19041	0.09570	0.14737	0.10325	0.10486
Global softness (s)	5.25183	10.44932	6.78564	9.68523	9.53652
Electronegativity (χ)	0.16572	0.16699	0.16933	0.16792	0.16418
Chemical potential (μ)	−0.16572	−0.16699	−0.16933	−0.16792	−0.16418
Global electrophilicity (ω)	0.07212	0.14569	0.09728	0.13655	0.12853

$$\mathrm{Cv} = 7.86518 + 0.22642T - 1.04187 \times 10^{-4}T^2$$
$$S = 66.43707 + 0.27654T - 7.74787 \times 10^{-5}T^2$$
$$G = 121.618 - 0.10527T - 8.13118 \times 10^{-5}T^2$$
$$H = 109.67521 + 0.03716T + 5.56473 \times 10^{-5}T^2$$

The thermodynamic data can be used to compute the other thermodynamic energies according to relationships of thermodynamic functions and estimate directions of chemical reactivity according to the second law of thermodynamics in thermo chemical field.

Natural bond orbital analysis

NBO analysis originated as a technique for studying hybridisation and covalence effects in polyatomic wave functions, based on local block eigenvector of the one-particle density matrix. It can be used to assign the hybridization of atomic lone pairs and of the atoms involved in bond orbital and to illustrate the deciphering of the molecular wave function, such as Lewis structures charge, bond order, bond type, hybridisation, resonance and donor–acceptor interactions.

The selected natural atomic orbitals (NAO), their occupancies and the corresponding energy of thiamethoxam were described in Table 5. The bonding concepts such as bond orbital occupancies, contribution from parent NBO, and the natural atomic hybrids were depicted in Table 6. The atom label and a hybrid label showing the hybrid orbital (sp^x) composition (the amount of s-character, p-character) of thiamethoxam molecule determined by B3LYP/6311++G (d, p) theoretical level. The occupancies of NBOs in thiamethoxam are reflecting their exquisite dependence on the chemical environment. For example, the bonding orbital for C6—O3 with 1.98817 electrons has 32.43% C6 character in a $sp^{3.59}$ hybrid and has 67.57% O3 character in a $sp^{2.65}$ hybrid orbital of thiamethoxam. The bonding orbital C8—N9 with 1.98087 electrons has 38.50% C8 character in a $sp^{2.00}$ hybrid and has 61.50% N9 character in a $sp^{1.87}$ hybrid orbital. The C24—Cl28 with 1.98842 electrons has 47.44% C24 character in a $sp^{2.53}$ hybrid and has 52.56% Cl28 character in a $sp^{4.82}$ hybridized orbital.

Global and local reactivity descriptors

Based on density functional descriptors, global chemical reactivity descriptors of compounds such as hardness (η), softness (S), chemical potential (μ), electronegativity (χ) and electrophilicity index (ω) as well as local reactivity descriptors as the Fukui function and the philicity have been defined [45–49]. Using Koopman's theorem for closed-shell compounds, η, μ, χ can be defined as:

$$\eta = (I - A)/2$$
$$\mu = -(I + A)/2$$
$$\chi = (I + A)/2$$
$$S = 1/\eta$$
$$I = -E_{\mathrm{HOMO}} \text{ and } A = -E_{\mathrm{LUMO}}$$

where I and A are the ionization potential and electron affinity of the compounds. Electron affinity refers to the capability of a ligand to accept precisely one. Softness is a property of compound that measures the extent of chemical reactivity. It is the reciprocal of hardness. χ is the Mulliken electronegativity, because of the fundamental relationship to the chemical potential, χ is quite different from Pauling's original meaning of electronegativity, which was a property of an atom in a molecule. Now χ is a property of the entire molecule [49]. Recently Parr et al. [45] have defined a new descriptor to quantity the global electrophilic power of the compound as electrophilicity index (ω), which defines a quantitative classification of the global electrophilic nature of a compound Parr et al. [45] have proposed electrophilicity index (ω) as a measure of energy lowering due to maximal electron flow between donor and acceptor. They defined electrophilicity index (ω) as follows

$$\omega = \mu^2/2\eta$$

The electrophilicity is a descriptor of reactivity that allows a quantitative classification of the global electrophilic nature of a molecule within a relative scale. The usefulness of this new reactivity quantity has been recently demonstrated in understanding the toxicity of various pollutants in terms of their reactivity and site selectivity [50–55]. All the calculated values of HOMO–LUMO, energy gap, ionization potential, Electron affinity, hardness, potential, softness and electrophilicity index are shown in Table 7.

Conclusions

Thiamethoxam was characterized by FT-IR, FT-Raman and UV–vis spectra. Vibrational frequencies were calculated using RHF and DFT method (B3LYP, CAMB3LYP, M06 and PBE1PBE) with 6-311++G (d, p) basis set. The observed frequencies are reproduced reasonably well by DFT methods, and DFT methods give more reasonable results than RHF method. The calculated frequencies deviations from the observed values are large for RHF frequencies. The predicted electronic absorption spectra were achieved by TDDFT in gas phase and PCM–TDDFT in H_2O solution. The calculated the strongest band centered at 211.8 and 238.8 nm in gas phase is closely agreement with the experimental one. The temperature dependence of thermodynamic parameters in the range of 100–1000 K was determined. The bond orbital occupancies, contribution from parent NBO; the natural atomic hybrids were discussed. The other molecular properties such as such as hardness (η), softness (S), chemical potential (μ), electronegativity (χ) and electrophilicity index (ω) were described.

Acknowledgment

We thank the National Science Foundation of Educational Commission of Jiangsu Province of China (Nos. 12KJA150004) for financial support.

References

[1] S. Kagabu, R. Ishihara, J. Agric. Food Chem. 55 (2007) 812–818.
[2] C.W. Sun, J. Zhu, Eur. J. Med. Chem. 46 (2011) 11–20.
[3] Z.Z. Tian, X.S. Shao (Eds.), J. Agric. Food Chem. 55 (2007) 2288–2292.
[4] M. Tomizawa, D.L. Lee, J.E. Casida, J. Agric. Food Chem. 48 (2000) 6016–6024.
[5] S.J. Lee, M. Tomizawa, J.E. Casida, J. Agric. Food Chem. 51 (2003) 2646–2652.
[6] M. Tomizawa, J.E. Casida, Annu. Rev. Pharmacol. Toxicol. 45 (2005) 247.
[7] T. Iwasa, N. Motoyama, J.T. Ambrose, R.M. Roe, Crop Prot. 23 (2004) 371–378.
[8] W. Xie, C. Han, Y. Qian, J. Chromatogr. A 1218 (2011) 4426–4433.
[9] T. Xu, Q.G. Xu, H. Li, J. Wang, Q.X. Li, W.L. Shelver, J. Li, Talanta 101 (2012) 85–90.
[10] W. Wakil, T. Riasat, J.C. Lord, J. Stored Products Res. 52 (2013) 28–35.
[11] I. Yamamoto, J. E. Casida, Springer, Tokyo, 1999, p. 49.
[12] P. Maienfisch, H. Huerlimann, Pest Manage. Sci. 57 (2001) 165–176.
[13] P. Maienfisch, M. Angst, Pest Manage. Sci. 57 (2001) 906–913.
[14] P. Jeschke, R. Nauen, J. Agric. Food Chem. 59 (2011) 2897–2908.
[15] S.H. Thany, Neuropharmacology 60 (2011) 587–592.
[16] Y. Benzidane, S. Touinsi, Pest Manage. Sci. 66 (2010) 1351–1359.
[17] Y.T. Feng, Q.J. Wu, Pest Manage. Sci. 66 (2010) 313–318.
[18] K.J.A. Rodrigues, M.B/ Santana, Ecotoxicol. Environ. Saf. 73 (2010) 101–107.
[19] G.J. Pandey, S.J. Dorrian, Biochem. Biophys. Res. Commun. 380 (2009) 710–714.
[20] H. Wellmann, M. Gomes, Pest Manage. Sci. 60 (2004) 959–970.
[21] Z.J. Papp, Serb. Chem. Soc. 75 (2010) 681–687.
[22] A. Pozzebon (Ed.), Pest Manage. Sci. 67 (2011) 352–359.
[23] R. Karmakar, G. Kulshrestha, Pest Manage. Sci. 65 (2009) 931–937.
[24] H.J. Kim (Ed.), Anal. Chim. Acta 571 (2006) 66–73.
[25] HyperChem Pro. Release 6.03, Hypercube Inc. USA, 2000.
[26] A.D. Becke, J. Chem. Phys. 98 (1993) 5648–5655.
[27] T. Yanai, D. Tew, N. Handy, Chem. Phys. Lett. 393 (2004) 51–57.
[28] Y. Zhao, D.G. Truhlar, Theor. Chem. Acc. 120 (2008) 215–241.
[29] C. Adamo, V. Barone, J. Chem. Phys. 110 (1999) 6158–6169.
[30] A.D. Becke, J. Chem. Phys. 98 (1993) 5648–5652.
[31] C. Jarmorski, M.E. Casida, D.R. Salahub, J. Chem. Phys. 104 (1996) 5134–5147.
[32] R. Cammi, J. Tomasi, J. Comput. Chem. 16 (1995) 1449–1458.
[33] M.J. Frisch, G.W. Trucks, H.B. Schlegel, GAUSSIAN 09, Revision B.03, Gaussian, Inc., Pittsburgh PA. 2009.
[34] N. Sundaraganesan, S. Kalaichelvan, J. Cornard. Spectrochim. Acta 71 (2008) 898–906.
[35] S. Gunasekaran, K. Rajalakshmi, Subramanian Kumaresan, Spectrochim. Acta Part A: Molec. Biomolec. Spectrosc. 112 (2013) 351–363.
[36] M.A. Makhyoun, R.A. Massoud, S.M. Soliman, Spectrochim. Acta Part A: Molec. Biomolec. Spectrosc. 114 (2013) 394–403.
[37] V. Krishnakumar, N. Surumbarkuzhali, S. Muthunatesan, Spectrochim. Acta A 71 (2009) 1810–1813.
[38] E. Vessally, E. Fereyduni, H. Shabrendi, M. Esrafili, Spectrochim. Acta Part A: Molec. Biomolec. Spectrosc. 116 (2013) 65–73.
[39] P. Alcolea, M. Rastogi, V.K. Mittal, Int. J. Quantum Chem. 94 (2003) 189–204.
[40] N. Sundaraganesan, B.D. Joshua, T. Radjakoumar, India J. Pure Appl. Phys. 47 (2009) 248–258.
[41] H. Roohi, A.R. Nowroozi, E. Anjomshoa, Comput. Theor. Chem. 965 (2011) 211–220.
[42] P. Munshi, T.N. Guru Row, Acta Crystallogr. B62 (2006) 612–626.
[43] S. Mebs, A. Luth, P. Luger, Bioorg. Med. Chem. 18 (2010) 5965–5974.
[44] J.B. Ott, J.B. Goates, Calculations from Statistical Thermodynamics, Academic Press, 2000.
[45] R.G. Parr, L.V. Szentpaly, S.J. Liu, Am. Chem. Soc. 121 (1999) 1922–1929.
[46] P.K. Chattraj, B. Maiti, U.J. Sarkar, J. Phys. Chem. A 107 (2003) 4973–4981.
[47] R.G. Parr, R.A. Donnelly, J. Am. Chem. Soc. 68 (1978) 3807–3816.
[48] R.G. Parr, R.G. Pearson, J. Am. Chem. Soc. 105 (1983) 751–759.
[49] R.G. Pearson, J. Chem. Sci. 117 (2005) 369–377.
[50] R. Parthasarathi, J. Padmanabhan, J. Phys. Chem. A 107 (2003) 10346.
[51] P. Thanikaivelan, V. Subramanian, Chem. Phys. Lett. 59 (2000) 323.
[52] R. Parthasarathi, J. Padmanabhan, Curr. Sci. 86 (2004) 535.
[53] R. Parthasarathi, J. Padmanabhan, Chattaraj (Eds.), Internet Electron J. Mol. Des. 2 (2003) 798.
[54] R. Parthasarathi, V. Subramanian, Bioorg. Med. Chem. 12 (2004) 5533–5543.
[55] R. Parthasarathi, J. Padmanabhan, Chem. Phys. Lett. 394 (2004) 225.